Supplement of Atmos. Chem. Phys., 19, 11363–11382, 2019
https://doi.org/10.5194/acp-19-11363-2019-supplement

Atmospheric Chemistry and Physics
Open Access

Supplement of

Over a 10-year record of aerosol optical properties at SMEAR II

Krista Luoma et al.

Correspondence to: Krista Luoma (krista.q.luoma@helsinki.fi) and Aki Virkkula (aki.virkkula@fmi.fi)

S1. Data coverage

The data coverage for each month is presented in Table S1. The data coverage is presented separately for σ_{sca} and σ_{abs}. The Table S1 shows clearly how the data coverage improved from the beginning of the measurements to 2017. The data was quality assured by the author. Data was invalidated if the instrument had mechanical problems or if the RH in the istrument exceeded 40 %.

Table S1. Data coverage of the extensive AOPs. The data coverage is presented as percentages for each month.

Data coverage (%)		Jan	Feb	Mar	Apr	May	Jun	Jul	Aug	Sep	Oct	Nov	Dec
2006	σ_{sca}	-	-	-	-	-	29	54	25	28	64	99	42
	σ_{abs}	-	-	-	-	-	27	52	25	27	64	100	43
2007	σ_{sca}	0	54	100	99	76	81	3	9	46	51	71	89
	σ_{abs}	0	53	99	99	76	81	2	08	46	58	83	91
2008	σ_{sca}	100	99	100	93	99	45	14	10	57	68	98	97
	σ_{abs}	99	96	100	92	99	44	13	10	55	67	97	98
2009	σ_{sca}	100	100	100	100	34	0	0	15	33	83	97	93
	σ_{abs}	97	99	100	100	38	0	0	14	32	85	98	89
2010	σ_{sca}	100	97	28	0	0	76	93	92	100	15	0	56
	σ_{abs}	86	80	28	0	0	77	92	90	100	15	0	57
2011	σ_{sca}	96	98	87	79	84	90	31	85	100	84	100	97
	σ_{abs}	76	0	74	100	98	100	63	100	100	85	100	92
2012	σ_{sca}	98	99	99	100	100	97	98	100	98	100	100	93
	σ_{abs}	98	100	99	100	82	28	0	0	0	0	0	0
2013	σ_{sca}	97	51	79	100	100	100	100	100	100	100	100	96
	σ_{abs}	0	0	79	100	100	100	100	100	99	99	99	89
2014	σ_{sca}	77	92	98	100	100	100	100	100	100	100	100	97
	σ_{abs}	70	91	98	100	100	99	100	100	100	99	100	0
2015	σ_{sca}	100	100	100	100	100	100	100	100	100	99	41	69
	σ_{abs}	0	0	0	0	89	95	100	99	100	91	43	69
2016	σ_{sca}	100	100	100	100	100	100	100	84	100	100	100	97
	σ_{abs}	94	100	100	99	99	100	100	87	99	100	100	100
2017	σ_{sca}	100	100	100	92	100	100	100	98	100	100	100	38
	σ_{abs}	100	100	99	65	95	99	99	96	100	100	81	14

S2. Seasonal environmental variables for calculating the RFE

The seasonal variability of the environmental parameters (D, R_S, A_C, and RH) used in calculating the seasonal radiative effective forcing (RFE_S and $RFE_{S,moist}$) are presented in Fig. S1. The fractional daylength (D) was calculated for the latitude of 61°N and the seasonal variation of D is presented in Fig. S1a. The surface reflectance (R_S) was determined by using the surface reflectance measurements by Kuusinen et al., (2012) and the seasonal variation of R_S is presented in Fig. S1b. The cloud fraction was measured (A_C) by a ceilometer that was deployed to a nearby airport that is located about 25 km from SMEAR II. The monthly means were calculated by using data from 2010 to 2017 and the seasonal variation is presented in Fig. S1c. The relative humidity (RH) measurements were conducted with a RH sensor (Rotronic model MP102H) at 16 m height at SMEAR II. We used measurements from 2012 to 2017 in calculating the monthly means that are presented in Fig. S1d. For the D and R_S we used daily values and for the A_C and RH the monthly means were used in calculating the RFE

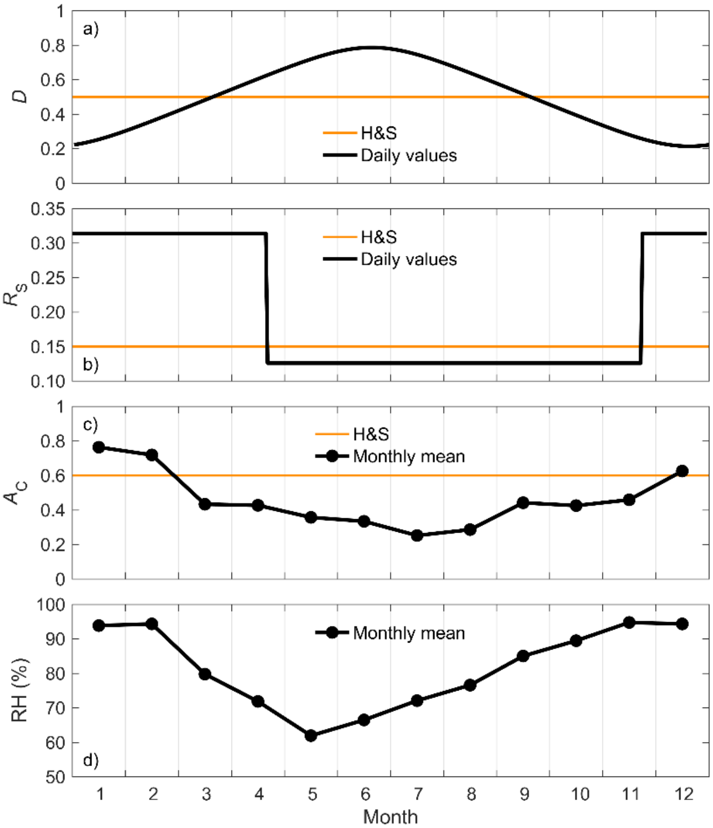

Figure S1: Seasonality of a) the fractional day length (D), b) the surface reflectance (R_S), c) the cloud fraction (A_C), and d) the relative humidity (RH). In calculating the RFE_S and $RFE_{S,moist}$, we used daily values for D and R_S, and monthly means for A_C and RH. The orange line represents the constant values suggested by Haywood and Shine (1995), which were used in calculating the $RFE_{H\&S}$.

S3. Aethalometer data processing

S3.1 Flow correction

The flow reported by the Aethalometer was corrected by using the weekly flow measurements conducted at SMEAR II with a Gilian flow meter. For correcting the flow we used a three-month moving average of the measured flow. The corrected flow is presented in Fig. S2.

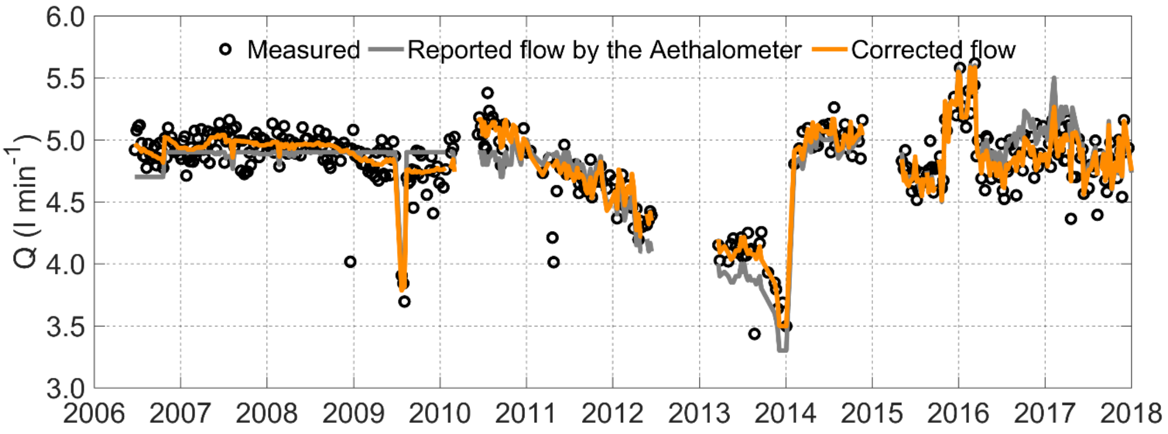

Figure S2: The Aethalometer flow (Q) correction. The black circles represent the flow measurements that were conducted almost every week at SMEAR II. The gray line is the flow that was reported by the Aethalometer and the orange line represents the corrected flow that was used in the data analysis.

S3.2 Difference between correction algorithms

In Table S2, we present values for PM10 AOPs that depend on the σ_{abs}. In Table S2, the absorption data was corrected with the correction algorithm that was suggested by Arnott et al., (2005) with a C_{ref} = 3.688 at λ = 520 nm in a similar manner to Virkkula et al. (2011). However, the results may vary from Virkkula et al., (2011), since we used a spot size correction and a flow correction.

By comparing Table S2 to the Table 1 in the main article, we see that there is no large difference between the measured σ_{abs} at 520 nm. Since the σ_{abs} is rather similar, there is no notable difference in ω_0 either. There is a larger difference, however, in σ_{abs} at other wavelengths. This causes the α_{abs} to be remarkably higher than the α_{abs} that was determined for data, which was corrected with the algorithm described in the main article. We also did the trend analysis for the data corrected with the algorithm by Arnott et al., (2005). The slope of the σ_{abs} statistically significant trend was -0.085 Mm^{-1}yr^{-1} (-6 %yr^{-1}), which was similar to the trend determined with the new algorithm by Collaud Coen et al., (2010).

Table S2. PM10 AOPs derived from Aethalometer data that was corrected with the algorithm described by Arnott et al. (2005).

PM10	λ (nm)	mean ± SD	1 %	10 %	25 %	50 %	75 %	90 %	99 %
σ_{abs} (Mm^{-1})	370	3.3 ± 3.9	0.2	0.6	1.1	2.1	4.1	7.3	19.4
	520	2.1 ± 2.4	0.1	0.4	0.7	1.4	2.6	4.7	12.0
	950	1.0 ± 1.1	-0.1	0.1	0.3	0.6	1.2	2.2	5.3
ω_0	450	0.88 ± 0.08	0.63	0.79	0.84	0.89	0.93	0.95	0.99
	550	0.87 ± 0.09	0.62	0.78	0.84	0.89	0.92	0.95	0.99
	700	0.85 ± 0.09	0.56	0.75	0.81	0.87	0.91	0.95	0.99
α_{abs}	370/520	1.30 ± 0.60	0.16	0.85	1.10	1.30	1.46	1.68	2.86
	370/950	1.36 ± 0.51	0.28	0.92	1.16	1.34	1.49	1.71	3.31
	470/950	1.43 ± 0.63	0.12	0.98	1.23	1.40	1.55	1.81	3.86
$RFE_{H\&S}$ (Wm^{-2})	550	-22 ± 8	-33	-29	-27	-23	-19	-15	-3

S4. Uncertainty analysis

We determined the uncertainties for the intensive PM10 AOPs using the equations presented in the supplementary material by Sherman et al. (2015). The absolute and fractional uncertainties are presented in Table S3. Here we used fractional uncertainties of 9.2 %, 8.0 %, and 23 % for the PM10 σ_{sca}, σ_{bsca}, and σ_{abs}, respectively. Since the uncertainties depend on the measured values, we used the mean values presented in Table 1 of the main article.

Table S3: Uncertainties for different intensive AOPs. Fractional uncertainty is the absolute uncertainty divided by the mean value of the AOP. The uncertainties for ω_0, b, and $RFE_{H\&S}$ were determined at 550 nm. The uncertainty for α_{sca} was determined for the wavelength range 450–700 nm, and the uncertainty for the α_{abs} was determined for the wavelength range 370–950 nm.

	Absolute uncertainty	Fractional uncertainty (%)
$\Delta\omega_0$	0.018	2.1
Δb	0.003	2.2
$\Delta\alpha_{sca}$	0.044	2.5
$\Delta\alpha_{abs}$	0.26	27.7
$\Delta RFE_{H\&S}$ (Wm^{-2})	1.42	6.5

S5. Seasonality of the trends

Fig. S3 presents the time series of the σ_{sca}, σ_{abs}, V_{tot}, and V_{fine} monthly medians separately for spring, summer, autumn, and winter. Fig. S3 reveals the the year-to-year variablity between different seasons and it seems that in winter the variation from the fitted trend line is the highest. This is probably due to changes in the meteorological conditions. For example, according to the statistics provided by the FMI (FMI: http://ilmatieteenlaitos.fi/vuositilastot, in Finnish only, last access: 25 March 2019) winter 2008 (December 2007 – February 2008) was exeptionally warm and the air masses arriving to Finland were mostly from the South and South-West that explains the low concenrations. On the contrary, high concentrations were measured in winter 2010, which was according to the reports by the FMI notably colder than average. It also seems from Figs. S3c, h, and g that the concentration in winter increased from 2006 to 2010 after which it started to decrase. For other seasons we do not observe this kind of variation.

We did a similar analysis for the seasonal trends of V_{tot} and V_{fine} as we did for the σ_{sca} and σ_{abs} in the main article. The results are presented in Table S3. For V_{tot} we observed a significant decreasing trend for all seasons and for V_{fine} we observed significant trends for spring, summer, and winter. For the V_{tot} the relative trends were rather similar for all the seasons; the relative trends of V_{fine} had more variation between the seasons. The variation of V_{fine} relative trends was similar to that of the σ_{sca} and σ_{abs}; the trends were most negative in winter and spring, and least negative in summer. This analysis would suggest that the variation of the σ_{sca} and σ_{abs} seasonal trends was due to varying trends in fine particle concentration.

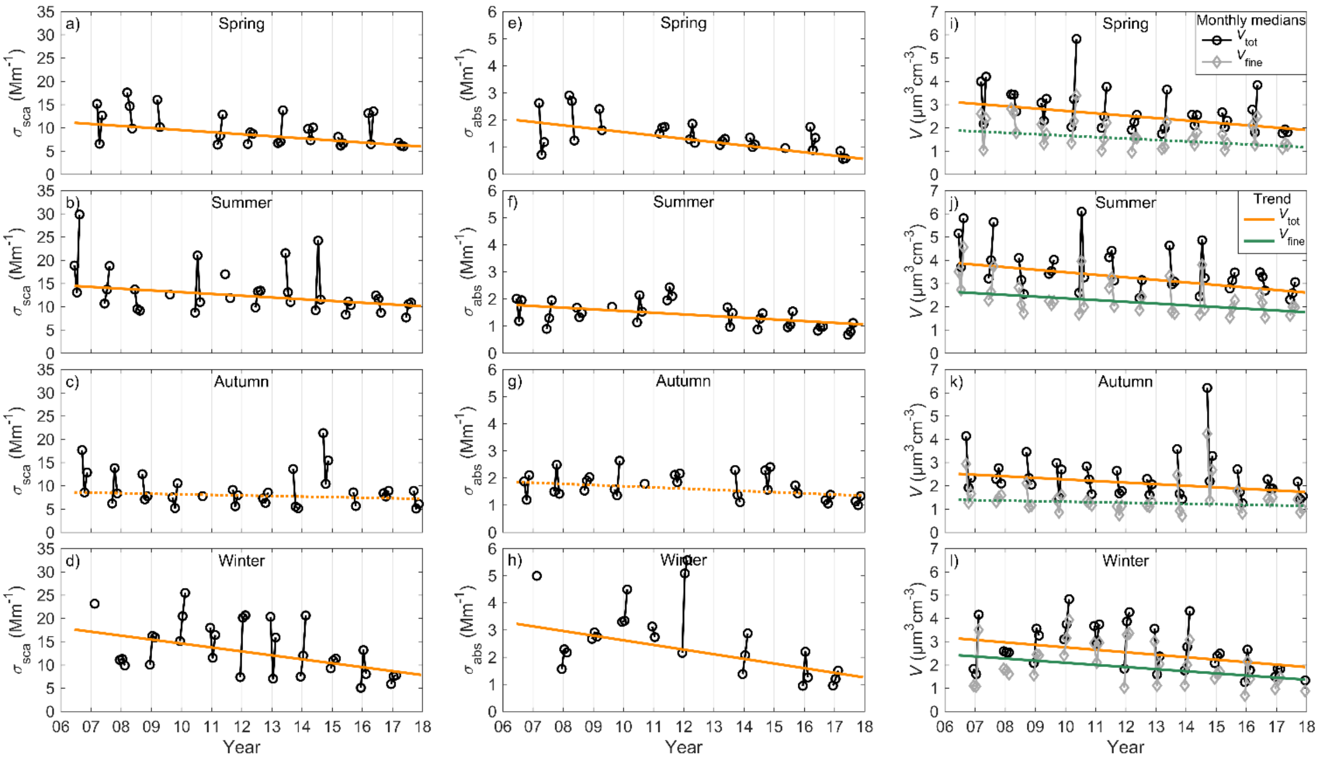

Figure S3: Monthly median values of a) – d) σ_{sca}, e) – h) σ_{abs}, and i) – l) V_{tot} (black) and V_{fine} (gray). and their trends. If the trend was statistically significant, the line is uniform and if the *p* value of the trend was > 0.05, the line is dashed.

Table S4: The seasonal trend for V_{tot} and V_{fine}.

	Trend (yr^{-1})		Lower (yr^{-1})	Upper (yr^{-1})	*p*-value	Trend (yr^{-1})		Lower (yr^{-1})	Upper (yr^{-1})	*p*-value
Spring	-0.10	-4 %	-0.20	-0.04	< 0.01	-0.06	-4 %	-0.15	0.00	0.07
Summer	-0.11	-3 %	-0.20	-0.03	< 0.01	-0.07	-3 %	-0.14	-0.02	< 0.01
Autumn	-0.07	-3 %	-0.11	-0.02	< 0.01	-0.02	-2 %	-0.07	0.01	0.23
Winter	-0.11	-4 %	-0.21	-0.01	< 0.05	-0.09	-5 %	-0.18	-0.00	< 0.05

S6. The trend of size distribution

The trend for the size distribution was determined by applying the seasonal Kendall test to each channel of the TDMPS and APS. The results are shown in Fig. S4 that presents statistically significant decreasing trends for most of the measurement channels. The relative trend was the most negative (about -5 % yr^{-1}) for particles that were about 500 – 800 nm in diameter. Fig. S6 shows that the particle volume size distribution typically has a peak around 200 – 400 nm so the largest decrease occurs on the larger side of the accumulation mode.

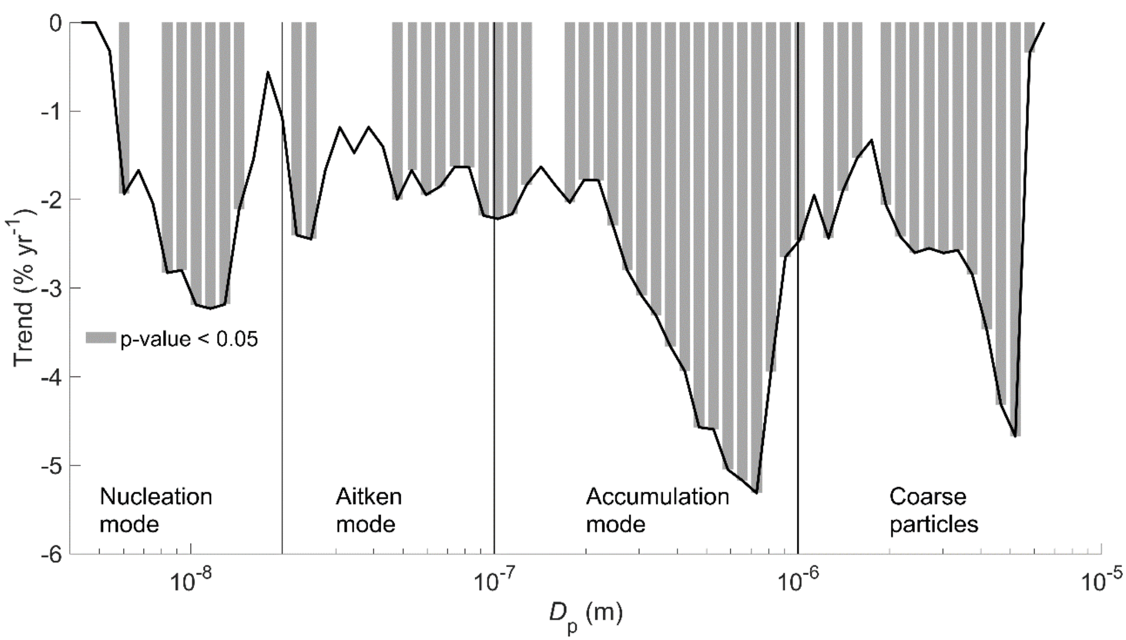

Figure S4: Trend analysis for the size distribution. The solid line represents the average trend in percentages. The gray bars mark the size ranges, in which the trend was statistically significant (*p*-value < 0.05). The typical borders of the nucleation, Aitken, accumulation and coarse particle modes are marked with vertical lines.

S7. The seasonal variation of the size distribution

Fig. S5 presents the seasonal variation of the geometrical mean diameter (GMD), the volume mean diameter for fine particles (D_p < 1 µm, VMD_{fine}) and the volume mean diameter for all particles (D_p < 10 µm, VMD_{tot}). The seasonal variation of the size distribution helps interpreting the seasonal variation of the σ_{sca} PM1/PM10 ratio, α_{sca} and b that are sensitive to different size ranges.

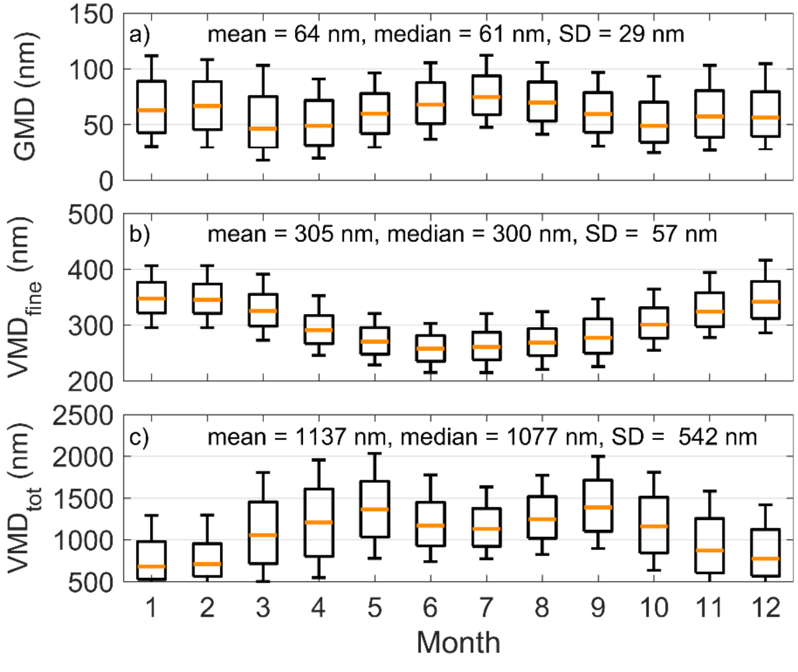

Figure S5: The seasonal variation and statistics for a) the GMD, b) the VMD_{fine}, and c) VMD_{tot}.

S8. Effect of exculding the moist data on the seasonal variation

Fig. S6 presents the monthly median values of different AOP for the dry data only and for a data set that included the moist data as well. The moist nephelometer data was corrected to dry conditions by using the equations and parameters presented in Sect. 2.3.1. Since the moist data occurred in summer and autumn, the difference between the different data sets is the highest from June to October.

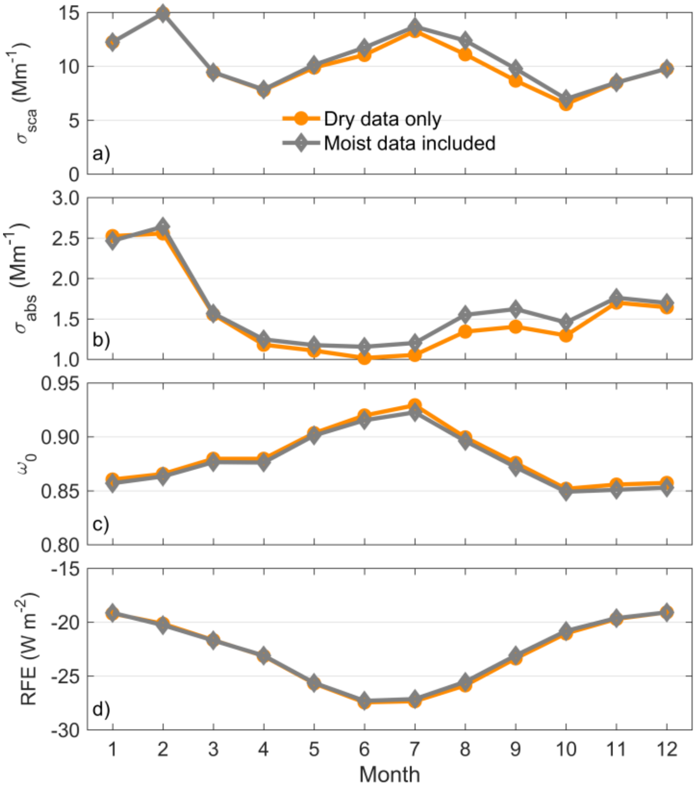

Figure S6: Monthly median values of a) σ_{sca}, b) σ_{abs}, c) ω, and d)RFE. The orange line presents the median values for the data set from where the moist periods before 2010 were excluded and the gray line reprents a data set where all the data were taken into account.